# Sideband cooling of the radial modes of motion of a single ion in a Penning trap

P. Hrmo,[*] M. K. Joshi ©,[†] V. Jarlaud ©,[‡] O. Corfield ©, and R. C. Thompson ©[§]

*Quantum Optics and Laser Science, Blackett Laboratory, Imperial College London, Prince Consort Road, London SW7 2AZ, United Kingdom*

Doppler and sideband cooling are long-standing techniques that have been used together to prepare trapped atomic ions in their ground state of motion. In this paper we study how these techniques can be extended to cool both radial modes of motion of a single ion in a Penning trap. We numerically explore the prerequisite experimental parameters for efficient Doppler cooling in the presence of an additional oscillating electric field to resonantly couple the radial modes. The simulations are supported by experimental data for a single $^{40}\mathrm{Ca}^+$ ion Doppler cooled to $\sim$100 phonons in both radial modes at a magnetron frequency of 52 kHz and a modified cyclotron frequency of 677 kHz. For these frequencies, we then show that mean phonon numbers of 0.35(5) for the modified cyclotron and 1.7(2) for the magnetron motions are achieved after 68 ms of sideband cooling.

## I. INTRODUCTION

Trapped ion systems provide an excellent platform for studying quantum-mechanical phenomena and performing high-precision measurements due to strong isolation from the environment, a high degree of control, and very good spatial confinement. The latter feature is predicated on the success of various cooling techniques to reduce the motional amplitude of the ions in the trap, allowing for long interaction times and reduced Doppler shifts. In particular, for certain ion species, laser-cooling techniques including resolved sideband, Raman, and electromagnetically induced transparency (EIT) methods have been able to cool single ions [1–4] or Coulomb crystals of a few to many ions to the quantum-mechanical ground state of motion [5–9]. In rf traps, the basic technique of a laser red-detuned from a dipole-allowed atomic resonance and passing through the trap center is sufficient for Doppler cooling of all three motional degrees of freedom of a single ion, enabling a subsequent period of sub-Doppler cooling to drive a desired mode to its ground state. This has allowed rf trap systems to establish themselves in the field of quantum information processing [10–12], quantum simulation [13–17], quantum optics [18], and ion clocks that employ quantum-logic spectroscopy [19].

In contrast, an ion in a Penning trap would be deconfined in the radial plane using this simple approach to Doppler cooling; instead, an offset beam geometry that uses a radial intensity gradient is required [20], resulting in an experimentally achievable parameter space that often leaves at least one of the radial motional modes with very high phonon numbers ($\bar{n} > 1000$, see Sec. II B) that are not amenable to ground-state

cooling techniques. For this reason, applications of Penning traps were historically mostly limited to instances where laser cooling was not required, such as mass spectrometry [21] or high-precision measurements of $g$ factors of electrons [22], protons [23], and antiprotons [24]. However, to increase the precision of these measurements even further, recent experiments are being pursued where laser-cooled ions are used to sympathetically cool molecular ions and highly charged atomic ions [25], protons, and antiprotons [26], and even to perform quantum-logic spectroscopy where the electronic state of (anti-)protons can be coherently mapped and read out using an atomic ion [27]. All these approaches stand to benefit from an improved understanding of Doppler and sub-Doppler laser-cooling techniques for the radial motion that will be discussed in this paper. Improved cooling also opens up potential avenues for high-fidelity quantum information experiments such as Ising model quantum simulations on a 2D ion Coulomb crystal with hundreds of ions [28,29] and implementations of error correction protocols [30]. These experiments have motivated a recent numerical study of Doppler cooling techniques for large crystals [31,32]. This paper complements these results by examining the case of a single ion.

This paper is split into two major sections. Section II aims to find experimental parameters for which both radial modes of motion can be Doppler cooled efficiently such that subsequent resolved sideband cooling can bring the ion to the radial ground state of motion. First, a brief theoretical summary of the motional mode description and analytical Doppler cooling models highlights the underlying difficulty of laser cooling in a Penning trap. Subsequently, the axialization technique for resonant mode coupling is introduced as a means to improve the cooling limits. Finally, numerical simulations are used to find cooling limits for a variety of experimental parameters, both with and without axialization.

The experimental results are then presented in Sec. III. After introducing the experimental setup, the Doppler cooling results and the effects of axialization are analyzed, showing that both radial modes can be cooled to $\sim$100 phonons. Lastly, sideband spectroscopy and Rabi oscillation data are used to

─────────
[*]Present address: Institute of Experimental Physics, University of Innsbruck, Innsbruck, Austria.

[†]Present address: Institute for Quantum Optics and Quantum Information, Austrian Academy of Sciences, Innsbruck, Austria.

[‡]Present address: Aarhus University, Aarhus, Denmark.

[§]r.thompson@imperial.ac.uk

demonstrate ground-state cooling of both modes of motion. Section IV concludes the paper with a brief summary and discussion of the results.

## II. DOPPLER COOLING THE RADIAL MOTION IN A PENNING TRAP

### A. Motion in a Penning trap

The classical motion of a single ion has been described in earlier works [33,34]. In this section, we will summarize the key results.

In an ideal Penning trap, a magnetic field $\mathbf{B} = B\hat{\mathbf{z}}$ is combined with a quadrupole electrostatic potential of the form

$$V(x, y, z) = \frac{V_0}{D_0^2}(2z^2 - x^2 - y^2), \quad (1)$$

where $D_0$ characterizes the geometric dimension of the trap and $V_0$ is the applied voltage. A particle with mass $M$ and charge $q$ will thus experience a force

$$M\ddot{\mathbf{r}} = q\dot{\mathbf{r}} \times \mathbf{B} - q\nabla V(\mathbf{r}). \quad (2)$$

The solutions of the equations of motions in terms of the Cartesian coordinates $(x, y, z)$ are

$$x(t) = r_- \cos(\omega_- t + \phi_-) + r_+ \cos(\omega_+ t + \phi_+), \quad (3a)$$

$$y(t) = -r_- \sin(\omega_- t + \phi_-) - r_+ \sin(\omega_+ t + \phi_+), \quad (3b)$$

$$z(t) = r_z \cos(\omega_z t + \phi_z), \quad (3c)$$

resulting in three motional modes with amplitudes $r_\pm$, $r_z$ and phases $\phi_\pm$, $\phi_z$, which depend on the initial conditions of position and velocity. The presence of the **B** field couples the motion in the radial $xy$ plane, resulting in mode frequencies

$$\omega_\pm = \frac{1}{2}\left(\omega_c \pm \sqrt{\omega_c^2 - 2\omega_z^2}\right) = \frac{\omega_c}{2} \pm \omega_1, \quad (4)$$

where $\omega_c = qB/M$ is the true cyclotron frequency and $\omega_1 = \sqrt{\omega_c^2 - 2\omega_z^2}/2$. In the radial plane, the particle thus undergoes a superposition of circular motions at the modified cyclotron $\omega_+$ and magnetron $\omega_-$ frequencies, whereas in the axial ($z$) direction the motion is simple harmonic with frequency $\omega_z = \sqrt{4qV_0/(MD_0^2)}$. The stability limit of the trap is set by $\sqrt{2}\omega_z \leqslant \omega_c$ such that the frequencies in Eq. (4) remain real. This implies that for a given magnetic field, the applied voltage is limited to $V_0 \leqslant qD_0^2 B^2/(8M)$.

Next, we find the cycle-averaged kinetic energy and potential energy using the results from Eq. (3):

$$\langle E_K \rangle = \left\langle \frac{1}{2}M\dot{\mathbf{r}}^2 \right\rangle = \frac{1}{2}M\left(\frac{1}{2}r_z^2\omega_z^2 + r_+^2\omega_+^2 + r_-^2\omega_-^2\right), \quad (5)$$

$$\langle E_V \rangle = \langle qV \rangle = \frac{1}{4}M\omega_z^2\left(r_z^2 - r_+^2 - r_-^2\right). \quad (6)$$

The total energy of motion is thus the sum of Eqs. (5) and (6):

$$\langle E_T \rangle = \frac{1}{2}M\left(r_z^2\omega_z^2 + 2r_+^2\omega_+\omega_1 - 2r_-^2\omega_-\omega_1\right). \quad (7)$$

From Eq. (7) we see that the term with the magnetron frequency is negative. This means that any reduction in the amplitude, and hence the kinetic energy, of the magnetron mode $r_-$ actually increases the total energy. Furthermore, the motion is now also unstable against perturbations, such as background gas collisions, that increase $r_-$. Thus to effectively cool the

particle, defined as a reduction of its kinetic energy irrespective of the total energy, the magnetron mode of motion will require a cooling mechanism that does not simply dissipate energy. The implications of this will be further discussed in the next section.

The quantized motion of the Penning trap can be formulated by imposing the canonical commutation relations $[\hat{q}_i, \hat{p}_j] = i\hbar\delta_{ij}$ on the classical canonically conjugate variables $q_i$ and $p_j$. Using an appropriate coordinate transformation [34–36], the Hamiltonian takes the form of three uncoupled harmonic oscillators,

$$\hat{H} = \hbar\omega_z\left(\hat{n}_z + \tfrac{1}{2}\right) + \hbar\omega_+\left(\hat{n}_+ + \tfrac{1}{2}\right) - \hbar\omega_-\left(\hat{n}_- + \tfrac{1}{2}\right), \quad (8)$$

in terms of the number operators $\hat{n}_z, \hat{n}_+, \hat{n}_-$ for the axial, modified cyclotron and magnetron modes, respectively. By defining $r_0 = \sqrt{\frac{\hbar}{M\omega_1}}$ and $z_0 = \sqrt{\frac{\hbar}{M\omega_z}}$ as the length scale of the ground-state wave packet of the radial and axial motion, respectively, and equating Eq. (7) to Eq. (8), the classical amplitude of motion can be related to the occupation number of each mode:

$$r_z^2 = 2z_0^2\left(n_z + \tfrac{1}{2}\right), \quad (9a)$$

$$r_+^2 = r_0^2\left(n_+ + \tfrac{1}{2}\right), \quad (9b)$$

$$r_-^2 = r_0^2\left(n_- + \tfrac{1}{2}\right). \quad (9c)$$

### B. Cooling theory

#### 1. Offset beam cooling

The simplest laser-cooling technique typically uses a laser beam that is red-detuned from a strong dipole-allowed atomic transition to create a velocity-selective damping force that removes energy from the particle. In the case of a harmonically trapped two-level particle in one dimension, photons are preferentially scattered when the ion is moving towards a laser beam parallel to the trap axis, as they come into resonance when the Doppler frequency shift approaches the laser detuning. After many such scattering events, the Doppler-limited temperature, assuming the photon emission to be isotropic, is given by [20]: $T = \hbar\Gamma/(3k_B)$, where $\Gamma$ is the transition linewidth and $k_B$ is the Boltzmann constant. In a multilevel system, such as the $^{40}$Ca$^+$ ion, the particle can decay to a long-lived metastable state from which it is returned back into the cooling cycle with the aid of an additional repump laser. The effect of this interaction, away from potential dark resonances, is taken to be small (e.g., $\sim$6% branching ratio in $^{40}$Ca$^+$) and for the purposes of this discussion ignored. For a harmonically bound particle in three dimensions in a Paul trap, a single laser aimed at the trap center with a projection onto all principal axes of motion is sufficient to cool all modes of motion. In a Penning trap, the same geometry would cool the axial $\omega_z$ mode and the radial $\omega_+$ modified cyclotron mode while heating the $\omega_-$ magnetron mode. This is a direct consequence of the negative total energy seen in Eq. (7), which causes a sign reversal in the rate of change of kinetic energy between $\omega_+$ and $\omega_-$. Thus to cool the magnetron motion, a blue-detuned laser beam would be required, implying there is no frequency-selective force that can cool both modes simultaneously [37].
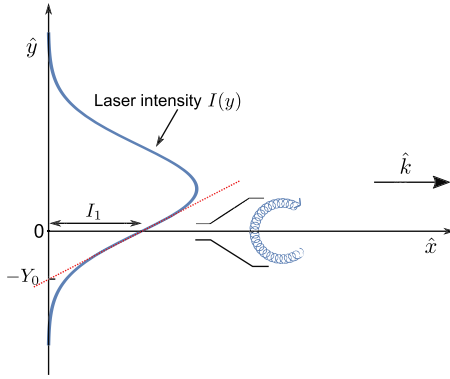
FIG. 1. Schematic diagram of the offset Doppler cooling beam relative to the ion trajectory in the trap. The clockwise trajectory is exaggerated for clarity.

To achieve simultaneous cooling of both radial modes, a spatial degree of freedom must be introduced whereby an inhomogeneous laser intensity profile breaks the symmetry around the center of the trap, leading to enhanced scattering when the ion is in the half of the magnetron orbit that moves away from the laser beam. Consider a typical laser beam with a Gaussian intensity profile:

$$I = \frac{2P_0}{\pi w_0^2} e^{-2(y-y_0)^2/w_0^2}, \tag{10}$$

with power $P_0$. Offsetting the beam waist $w_0$ from the trap center by $y_0$ creates a scattering rate gradient across the ion trajectory as shown in Fig. 1 and hence creates a position-dependent damping force for the magnetron motion. To facilitate an analytic derivation of the cooling limits, the beam intensity can be approximated as a linear function of the ion position $y$ giving $I(y) = I_1(1 + y/Y_0)$, with $I_1$ being the intensity at the trap center, provided that the ion orbit is small compared to the gradient parameter $Y_0$, i.e., $|y| \ll Y_0$. The largest gradient is obtained for an offset of $y_0 = w_0/2$; hence, for a given beam waist, the optimal gradient parameter is $Y_0 = w_0/2$. The initial theoretical analysis of Itano and Wineland [20] determined that to achieve simultaneous cooling of both modes an inequality must be obeyed:

$$\omega_- < \frac{(\Gamma/2)^2 + \delta^2}{2kY_0\delta} < \omega_+, \tag{11}$$

where $\Gamma$ is the transition linewidth, $\delta$ is the laser detuning (defined as positive below resonance), and $k$ is the wave number of the laser beam. This limit can be viewed as the parameter space for which simultaneous cooling of both modes can be obtained but does not constitute a hard cutoff since the approximation breaks down as the ion orbit grows. More recent analysis used numerical simulations to show that there are large amplitude steady states when accounting for the full laser profile [37]. It is also possible to derive analytical expressions for the cooling rates as a function of laser beam offset and detuning, including transition saturation effects [38]. Nonetheless, the resulting approximate mean phonon
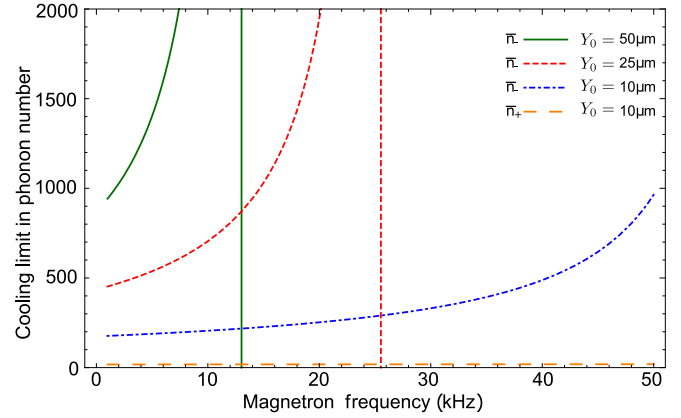


FIG. 2. Doppler cooling limit in terms of mean phonon number as a function of magnetron frequency for different beam offset parameters. The vertical lines for the red and green curves intersecting zero show the limit of cooling stability. Note that the modified cyclotron cooling limit response is almost flat even for a small offset parameter, in contrast with the rapid growth of the magnetron cooling limit for larger offset parameters.

number expressions at the Doppler limit remain useful and are given for both motions by [20]

$$\bar{n}_+ \approx \frac{5Y_0 k[(\Gamma/2)^2 + \delta^2]}{6\{2\delta\omega_+ Y_0 k - [(\Gamma/2)^2 + \delta^2]\}}, \tag{12}$$

$$\bar{n}_- \approx \frac{5Y_0 k[(\Gamma/2)^2 + \delta^2]}{6\{[(\Gamma/2)^2 + \delta^2] - 2\delta\omega_- Y_0 k\}}, \tag{13}$$

assuming no axial cooling beam and isotropic emission. An important thing to note from Eqs. (12) and (13) is that the sign of the position- and detuning-dependent terms in the denominator is reversed, showing the conflicting requirements on $\delta$ and $Y_0$ to minimize the respective mean phonon numbers. Furthermore, since $\omega_-$ can be up to 2 orders of magnitude smaller than $\omega_+$, the corresponding Doppler limit can be much higher. To illustrate this, Fig. 2 shows the Doppler limits at $\delta = \Gamma/2$ for a $^{40}$Ca$^+$ ion in the Imperial College Penning trap [39], operated at a magnetic field of 1.89 T. It is clear that to achieve sufficiently low mean phonon numbers of the magnetron motion at frequencies that are amenable to resolved sideband cooling, the $Y_0$ parameter needs to be as small as possible. For example, a mean phonon number of $\bar{n}_- \approx 200$ at $\omega_z = 2\pi \times 350$ kHz requires a beam waist of 20 $\mu$m. This is often in conflict with other experimental requirements. A tight waist is not suitable for initial cooling from large magnetron orbits and hence would greatly complicate the trap loading process. Even if an ion is successfully cooled to the trap center, any strong perturbation such as an elastic collision with a background gas molecule would leave the ion in a large orbit from which it cannot be efficiently recooled. Furthermore, a tight waist becomes very sensitive to beam pointing instabilities and makes it difficult to achieve a reproducible Doppler temperature without additional stabilization techniques. Lastly, a tight waist is also not suitable for cooling larger Coulomb crystals, which can have radii from tens to hundreds of micrometers. For these reasons, offset beam cooling alone is not sufficient to reach a suitably low

mean phonon occupation to enable sideband cooling to the ground state of the magnetron motion.

### 2. Axialization

In the previous section we showed that the two radial modes of motion can have vastly different Doppler cooling limits. One method to bridge this difference was originally proposed by Wineland and Dehmelt [40]: a resonant coupling between the axial and magnetron motion would lead to continuous exchange of energy between them, and if the cooling of the axial motion was faster than the heating of the magnetron motion, the two modes could be cooled simultaneously. This technique was initially demonstrated in a high-precision experiment which measured the anomalous magnetic moment of the electron in a Penning trap [41] and was later also applied to ions [42]. Similarly, a coupling between the modified cyclotron and magnetron motions can be achieved using an azimuthal quadrupolar field as produced with a ring electrode split into four segments [43]. This effect is achieved by applying an oscillating quadrupolar potential,

$$\phi_{ax} = \frac{V_a}{2R_0^2}(x^2 - y^2)\sin(\omega_c t), \quad (14)$$

with voltage $V_a$ at the true cyclotron frequency $\omega_c = \omega_+ + \omega_-$, to four equal segments of a ring electrode of effective radius $R_0$, with each neighboring segment phase shifted by $\pi$ radians. Combining this potential with the radial equations of motion, Eq. (2) yields

$$\ddot{u} + i\dot{u}\omega_c - \left(\frac{\omega_z^2}{2} - i\frac{qV_{ax}}{MR_0^2}\sin(\omega_c t)\right)u = 0, \quad (15)$$

where $u = x + iy$. This equation can be solved either by considering the instantaneous power absorption [44] or Green's functions [34,42]. The solutions yield a simple sinusoidal coupling at a rate

$$\Omega_a = \frac{qV_a}{4MR_0^2\omega_1}. \quad (16)$$

For a 1-V drive on a $^{40}$Ca$^+$ ion with $R_0 = 0.01$ m, $\omega_1 = 2\pi \times 300$ kHz, the coupling rate is $\Omega_a = 2\pi \times 500$ Hz, which is much slower than all the motional frequencies of the ion, allowing for a few complete energy exchange cycles during a typical Doppler cooling window (5–20 ms). In the presence of efficient damping of one of the modes (by laser cooling or otherwise), the axialization will drive the mean phonon numbers of the coupled modes towards equilibrium, $\bar{n}_+ = \bar{n}_-$ [34,45]. However, establishing the equilibrium value is not trivial.

Experimentally, the axialization technique has been shown to successfully cool the magnetron motion of $^{24}$Mg$^+$ ions [46,47] and single $^{40}$Ca$^+$ ions [8], in addition to clouds [48] and crystals [49,50], when compared to an offset beam-only method; however, no direct thermometry was performed. The thesis of Stutter [51] includes a brief study of a radial spectrum in the presence of axialization but observed high-order sideband excitations (8th–10th order) which were attributed to signatures of large driven motion orbits; hence no temperature was derived. Theoretical studies have so far focused on the cooling rates [52] without consideration of the final cooling limits. Recently, numerical simulations have investigated the cooling dynamics and limits in the presence of a uniform beam for a small array of six $^9$Be$^+$ ions in a honeycomb lattice [53]. In the following section we numerically investigate cooling limits for a single ion in the presence of axialization, including a nonuniform beam, and compare them with experimental results.

### C. Doppler cooling simulation and results

#### 1. Method

To investigate the cooling limits we numerically integrate the radial equations of motion [Eq. (15)] in the presence of stochastic momentum kicks from the cooling laser. To model the laser-ion interaction, we use a semiclassical model where we assume that a monochromatic laser photon with wave vector $\mathbf{k}$ will cause an instantaneous velocity change $\Delta\mathbf{v} = \hbar(\mathbf{k}' - \mathbf{k})/M$ of the ion after reemission with wave vector $\mathbf{k}'$. This approximation is valid, since the lifetime of the excited state of the cooling transition is much shorter than any of the oscillation periods of the ion motion. The laser linewidth is much smaller than the transition linewidth $\Gamma$, satisfying the monochromatic assumption, and the beam is normal to the magnetic field axis with $\mathbf{k} = k\hat{\mathbf{x}}$. The scattering rate, including the Doppler shift, is now given by

$$\gamma_g(t) = \frac{I(y)\sigma_0}{\hbar\omega_L}\frac{(\Gamma/2)^2}{(\Gamma/2)^2 + \frac{I(y)\sigma_0\Gamma}{2\hbar\omega_L} + (\delta + \dot{x}(t)k)^2}, \quad (17)$$

where $\sigma_0$ is the scattering cross section. In our experiment we address both $\sigma^\pm$ transitions with linear polarization perpendicular to the magnetic field and hence obtain $\sigma_0 = \lambda^2/(2\pi)$. The resulting excited-state population gives rise to an isotropic emission pattern when averaged over the decay path probabilities. Finally, we assume that the photon statistics are Poissonian and thus we can define a probability of scattering integer $n$ photons in a time interval $dt$ as $P_n(\gamma_g(t)dt)$.

The integration algorithm then proceeds as follows:

(1) Integrate the equations of motion [Eq. (2)] using an eighth-order Runge-Kutta method by a time step $dt$.

(2) Sample the Poissonian distribution $P_n(\gamma_g(t)dt)$ to find how many photons $n$ arrived in the time step.

(3) Generate $n$ uniformly distributed random vectors on a sphere of radius $k$ and sum them to find the total reemission wave vector $\mathbf{k}'$.

(4) Update the velocity coordinates by the corresponding velocity kicks:

$$\dot{x}(t) \rightarrow \dot{x}(t) + \frac{\hbar}{M}(kn + k'_x), \quad (18)$$

$$\dot{y}(t) \rightarrow \dot{y}(t) + \frac{\hbar}{M}k'_y. \quad (19)$$

The instantaneous square amplitudes of motion can be found by substituting the integrated coordinates into the cycle-averaged analytical square amplitudes:

$$\langle r_+^2\rangle = \frac{1}{4\omega_1^2}[(\omega_- x(t) + \dot{y}(t))^2 + (\omega_- y(t) - \dot{x}(t))^2], \quad (20)$$

$$\langle r_-^2\rangle = \frac{1}{4\omega_1^2}[(\omega_+ x(t) + \dot{y}(t))^2 + (\omega_+ y(t) - \dot{x}(t))^2]. \quad (21)$$

The mean phonon numbers can then be expressed in terms of the amplitudes as

$$\bar{n}_\pm = \frac{\langle r_\pm^2 \rangle M \omega_1}{\hbar}, \tag{22}$$

where we have neglected the zero-point energy. An important point to note is that the amplitudes are defined with respect to the center of the trapping potential; however, since the laser exerts a constant force in the $\hat{x}$ direction, it displaces the ion trajectory from the center, resulting in oscillatory values of $\langle r_+^2 \rangle$ and $\langle r_-^2 \rangle$ at the magnetron frequency $\omega_-$. If the cooling laser is turned off nonadiabatically, then the displacement is imprinted on the measured amplitude in each experimental realization depending on the phase of the oscillation. While this displacement increases or decreases the total with equal probability, the mean phonon number increases on average since it depends on the square of the displacement [Eq. (22)]. This process results in the creation of nonthermal, coherent states of motion. Since the magnitude of this heating varies with trap frequency and scattering rate, the position offset due to the constant force term, $2\hbar k \gamma_g(t_0)/(M\omega_z^2)$, is subtracted from the $x$ coordinates of the solution when calculating $\langle r_+^2 \rangle$ and $\langle r_-^2 \rangle$ to ensure consistency between simulated data sets. Experimentally, this heating process can be suppressed by turning off the cooling laser beam adiabatically with respect to the magnetron frequency.

The final issue to consider is how to extract equilibrium mean phonon values from the resulting trajectories. Given a particular set of parameters, a trajectory solution might show oscillatory behavior or very slow convergence to equilibrium. In a real experiment, cooling is typically performed for a fixed time period, after which spectroscopy would be performed. To restrict the simulation to realistic parameters that show fast dynamical convergence to the cooling limit, can overcome heating, and are robust at recooling ions that have collided with background particles, appropriate integration limits are chosen. The equations of motion are integrated for 20 ms, and the amplitudes are averaged over a 10–20-ms interval assuming that the ergodicity of a single trajectory gives us information about the average ensemble of amplitudes. The same initial conditions are used for all simulations: $x_i = -4 \times 10^{-6}$ m, $v_x = 1$ m s$^{-1}$, and $v_y = 2$ m s$^{-1}$. This corresponds to initial phonon numbers of $\bar{n}_- \approx 18\,250 \pm 150$, $\bar{n}_+ \approx 200 \pm 100$ across the simulated frequency range.

### 2. Results

We begin by showing the results of typical trajectory data used to extract equilibrium phonon numbers. In Fig. 3(a), the amplitudes of both motions are cooled by means of an offset Doppler beam without axialization. The modified cyclotron amplitude decreases rapidly within hundreds of microseconds, while the magnetron amplitude cools much slower and does not reach equilibrium in 20 ms. In Fig. 3(b), the modified cyclotron amplitude initially increases due to the effect of the 0.5 V axialization field, in addition to an offset Doppler beam, but the magnetron motion is cooled. These axialization-induced oscillations disappear once equilibrium is reached and the mean phonon number can once again be extracted by averaging over the 10–20 ms period where the
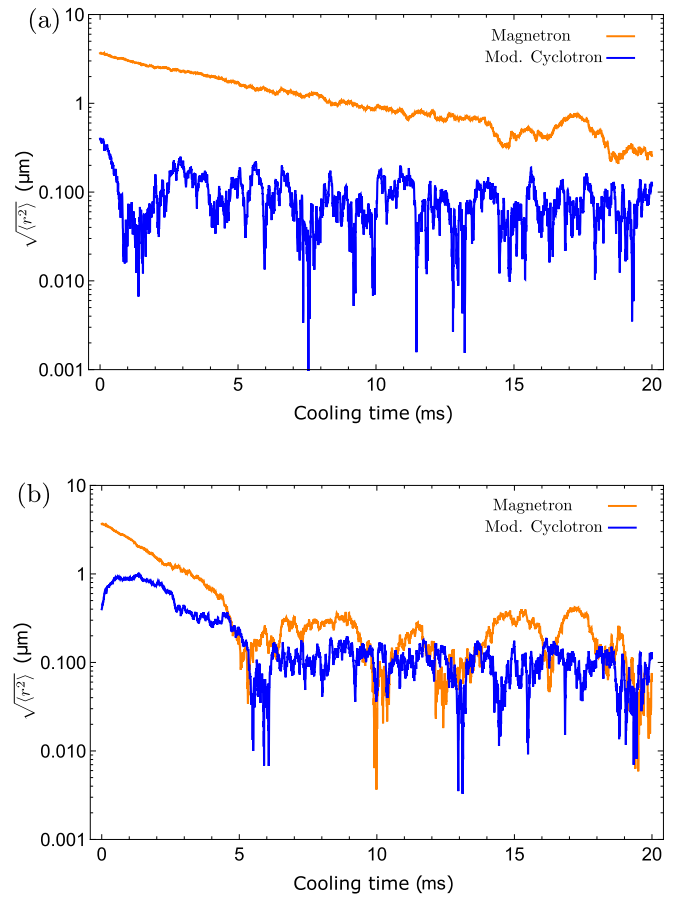


FIG. 3. Amplitudes of motion for the magnetron and modified cyclotron modes: (a) $V_a = 0$ V and (b) $V_a = 0.5$ V. In (b) the characteristic initial increase in the cyclotron amplitude due to the presence of the axialization drive is observed. This effect is absent in (a), where no axialization is present. Common parameters: $P_0 = 1\ \mu$W, $\delta = \Gamma/2$, $w_0 = 40\ \mu$m, $y_0 = 40\ \mu$m, $\omega_- = 2\pi \times 25$ kHz.

amplitude is dominated by random kicks from the photon scattering.

Based on the technique for extracting the equilibrium phonon numbers described above, the effect of cooling using axialization without an offset beam was investigated. Figure 4 plots various cooling limits as a function of the axialization voltage for different beam waists. First, note that at $V_{ax} = 0$ the magnetron motion is actively heated to very large orbits while the modified cyclotron motion remains relatively cold, consistent with the theoretical prediction that both modes cannot be cooled simultaneously. Furthermore, the larger scattering rate for smaller beam waists at the trap center leads to more efficient modified cyclotron cooling. As the axialization amplitude is increased, the magnetron mean phonon numbers start decreasing. The modified cyclotron mean phonon numbers initially increase, but with sufficient axialization the two values converge and approach a low total phonon number. It is clear that lower total mean phonon numbers can be obtained for larger beam waists, indicating that the broader beam waist contributes a larger net decrease in magnetron heating compared to the decrease in modified cyclotron cooling. Phonon numbers below 100 for both modes can be obtained with
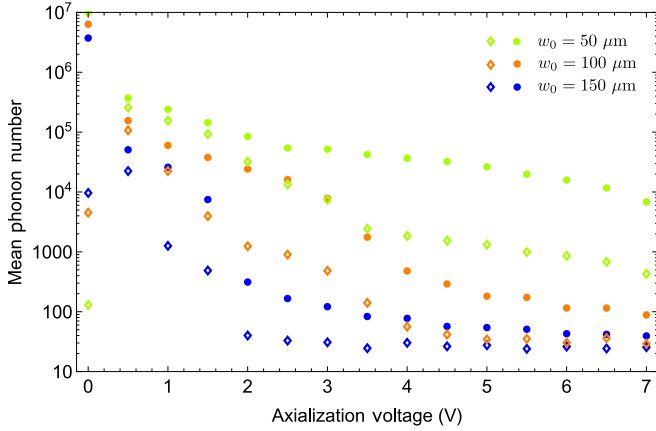
FIG. 4. Average phonon numbers for the magnetron (circles) and modified cyclotron (diamonds) motions between 10 and 20 ms as a function of axialization voltage for different beam waists. Parameters: $\omega_z = 2\pi \times 265$ kHz, $\omega_- = 2\pi \times 52$ kHz, $\omega_+ = 2\pi \times 677$ kHz, $y_0 = 0$ $\mu$m, $P_0 = 8$ $\mu$W, $\delta = \Gamma/2$. The axialization exchange rate $\Omega_a$ reaches $2\pi \times 3.5$ kHz at 7 V.

$V_{ax} > 3$ V and a beam waist of $w_0 = 150$ $\mu$m, which would be sufficient to enable sideband cooling. The disadvantage of using voltages in this range is that motion at the frequency of the axialization drive can become significant if stray fields and potential differences between the axialization voltages on different electrodes are not carefully compensated.

An alternative is to combine the axialization field with an offset Doppler cooling beam, as shown in Fig. 5 for two different beam waists. In this case, the axialization voltage required to achieve similar mean phonon numbers is an order of magnitude lower. Above $V_{ax} \approx 0.7$ V the effect of increased amplitude begins to saturate and the final mean phonon numbers of both modes are almost equalized. The phonon
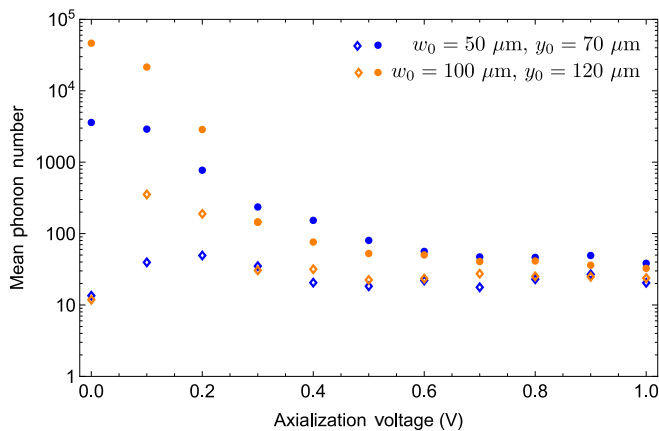


FIG. 5. Average phonon numbers for the magnetron (circles) and modified cyclotron (diamonds) motions between 10 and 20 ms as a function of axialization voltage for different beam waist and offset combinations. The offset was chosen to minimize the mean phonon numbers given the beam waist and power based on additional simulations at $V_{ax} = 0.5$ V. Parameters: trap potential 100 V, $\omega_z = 2\pi \times 265$ kHz, $\omega_- = 2\pi \times 52$ kHz, $\omega_+ = 2\pi \times 677$ kHz, $P_0 = 8$ $\mu$W, $\delta = \Gamma/2$.

numbers are within a factor of 3–4 larger than the modified cyclotron mean phonon number without axialization. Additionally, the benefits of a tighter beam waist are also evident at lower axialization voltages.

Further simulations using axialization voltages of $V_{ax} = 0.5$ and 1 V show that the mean phonon numbers of the two motions are almost equalized at values between 10 and 200 phonons at magnetron frequencies from $\omega_- = 2\pi \times 10$ to $\omega_- = 2\pi \times 190$ kHz. This very weak dependence on the applied dc endcap voltage suggests that with sufficient axialization voltage, efficient cooling is possible across the whole range of stable trap parameters.

## III. EXPERIMENTAL RESULTS OF DOPPLER AND SIDEBAND COOLING

### A. Experimental setup

The experiments performed in this paper are realized on a single $^{40}$Ca$^+$ ion confined in a cylindrical, stacked electrode Penning trap, in a vertical 1.89-T axial magnetic field (described in more detail in [39]). Voltages applied to the endcap electrodes provide axial confinement, while the central ring electrode is held at dc ground. This ring is split into four segments to enable application of ac voltages in order to generate the axialization field used for coupling the radial modes of motion. To apply the axialization potential to the electrodes, a single frequency at $\omega_c = 2\pi \times 729$ kHz is generated and split into four paths, where the appropriate phase shifts are applied using variable-gain op-amp circuits.

Doppler cooling is performed using two diode lasers at 397 nm, tuned to the $S_{1/2,-1/2} \leftrightarrow P_{1/2,+1/2}$ and $S_{1/2,+1/2} \leftrightarrow P_{1/2,-1/2}$ transitions which are split by $\sim 20$ GHz due to the magnetic field. The two lasers are linearly polarized and have independent frequency control but are typically set to have the same detuning from resonance. The combined light is split into two paths, one parallel to the magnetic field to cool the axial motion and one perpendicular to the magnetic field (polarized in the plane perpendicular to the magnetic field) to cool the radial motion. The two paths have independent intensity control but are restricted to having the same frequency. The radial beam position relative to the ion is controlled using a piezo-controlled mirror mount with a CCD camera to track the position. The waist of the radial beam is approximately $w_0 \approx 100$ $\mu$m. Repumping beams at 866 and 854 nm are passed through a fiber electro-optical modulator to generate the necessary frequencies to clear out all Zeeman sublevels of both the $D_{3/2}$ state and also the $D_{5/2}$ state, which is populated due to weakly allowed decay from the $P_{1/2}$ state at high magnetic field [54].

Coherent addressing is performed on the $S_{1/2,-1/2} \leftrightarrow D_{5/2,-3/2}$ transition with a narrow linewidth ($< 1$ kHz) laser at 729 nm with $\hat{\mathbf{k}} = \hat{x}$ and linear polarization perpendicular to the magnetic field. The laser frequency is controlled by means of a single-pass acousto-optic modulator driven by a single direct digital synthesizer (DDS) which can dynamically switch between up to eight frequencies during an experimental cycle, allowing for sideband cooling sequences involving multiple higher-order sidebands. The 854-nm laser is also used during
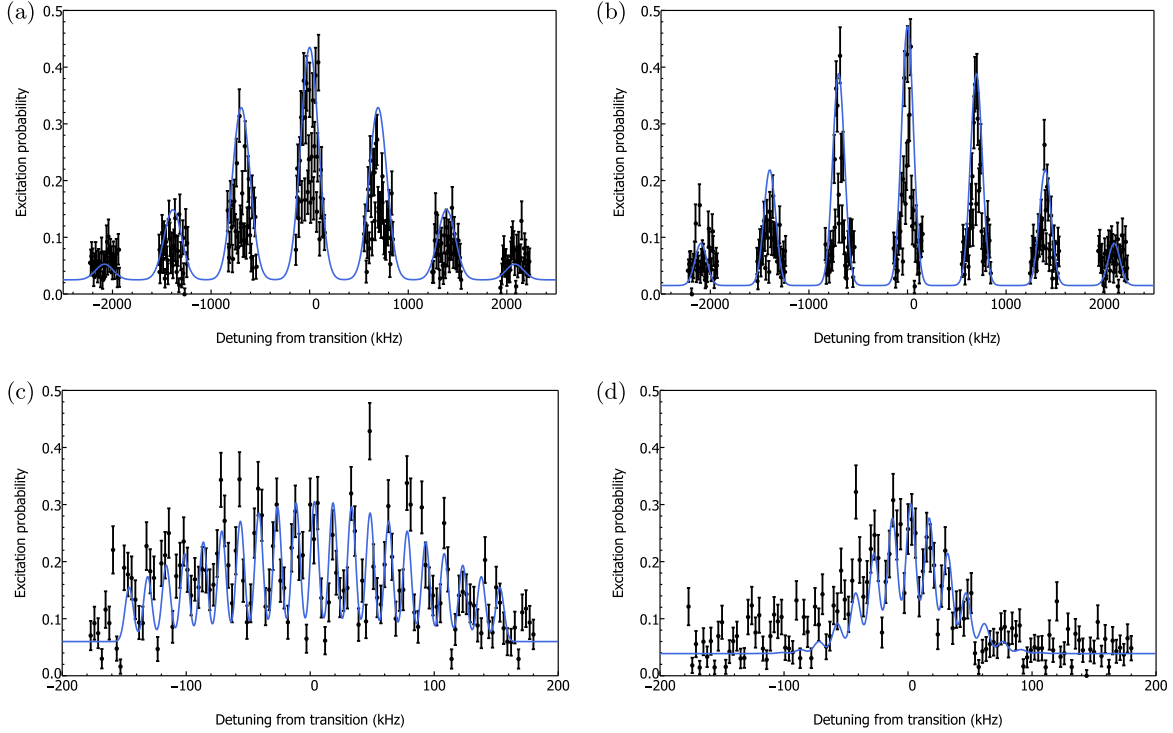
FIG. 6. Radial spectra of a single ion after Doppler cooling at $\omega_+ = 2\pi \times 693$ kHz, $\omega_- = 2\pi \times 14.8$ kHz. The average occupation obtained from matching the data to a comb of Gaussian sidebands modulated by a Gaussian envelope: from (a) and (b) $\bar{n}_+ \approx 31$ and $\bar{n}_+ \approx 45$, and from (c) and (d) $\bar{n}_- \approx 900$ and $\bar{n}_- \approx 100$, respectively. (a), (c) axialization off and (b), (d) 500 mV of axialization rf is applied. All other radial laser parameters are kept the same between figures: $\delta \approx \Gamma/2$, $w_0 \approx 100\ \mu$m, $y_0 \approx 80 - 120\ \mu$m.

the sideband cooling process to quench the $D_{5/2}$ state lifetime and thus increase the cooling rate.

State preparation is accomplished by optically pumping into the $S_{1/2,-1/2}$ state using the $S_{1/2,+1/2} \leftrightarrow P_{1/2,-1/2}$ laser. State detection uses the standard electron-shelving technique, with fluorescence collected on the 397-nm transition and imaged onto a pair of fibers coupled to photomultiplier tubes with typical detection times of 12 ms. Decays from the $P_{1/2}$ state to the $D_{5/2}$ state induce approximately 4% of shelving background when using a threshold to discriminate between the states. This error is currently limited by the total collection efficiency of 0.04%, which sets a lower bound on the readout time. Each experimental cycle of cooling, probe, and detection is repeated 100 times at a single frequency for the Doppler data and 200 times at a single probe time for the Rabi data.

### B. Experimental results

#### 1. Doppler cooling

In order to extract a temperature for the ion after Doppler cooling, we use a fixed length probe and scan the 729-nm laser frequency to obtain excitation strengths of the spectral components of the two radial modes of motion. This approach allows us to decouple the contributions of the two different modes of motion, which would not be possible using Rabi oscillations on the carrier. In the interest of comparing the performance of cooling with and without axialization, we must work in a regime where offset beam Doppler cooling still yields a stable and measurable $n_-$ value, which restricts us to working with very low magnetron frequencies on the order of $\omega_z =$

$2\pi \times 5 - 15$ kHz. However, due to the density of spectral features, where sets of low-frequency magnetron sidebands modulate a wide comb of modified cyclotron sidebands, a fit to the full spectral line shape summed over the motional Fock states of motion becomes unfeasible. Instead, we extract the temperatures of both modes by measuring the spectral width of the sideband structure of each mode from separate scans using different frequency sampling. The data is modeled as a comb of Gaussian peaks modulated by a Gaussian envelope with linewidth $\sigma_\pm$, which defines the temperature as

$$T_\pm = \frac{M\lambda_{729}^2 \sigma_\pm^2}{k_B}, \tag{23}$$

where $\lambda_{729}$ is the transition wavelength. The mean occupation numbers can then be obtained:

$$\bar{n}_\pm = \frac{T_\pm k_B \omega_1}{2\hbar\omega_\pm^2}. \tag{24}$$

Using the approach described above, Fig. 6 compares the mean phonon numbers after 10 ms of Doppler cooling with and without axialization. First, panel (a) exhibits modified cyclotron sidebands at 693 kHz, modulated at 15 kHz by magnetron sidebands which are not fully resolved. The estimated Doppler temperature of the modified cyclotron motion is within a factor of 2 of the Doppler limit. When we zoom in on the carrier, shown in panel (c), we see at least ten magnetron sidebands, which corresponds to a magnetron mean phonon number of approximately $\bar{n}_- \approx 900$. Applying an axialization drive of $V_{ax} = 0.5$ V greatly suppresses the number of magnetron sidebands in panel (d), reducing $\bar{n}_-$
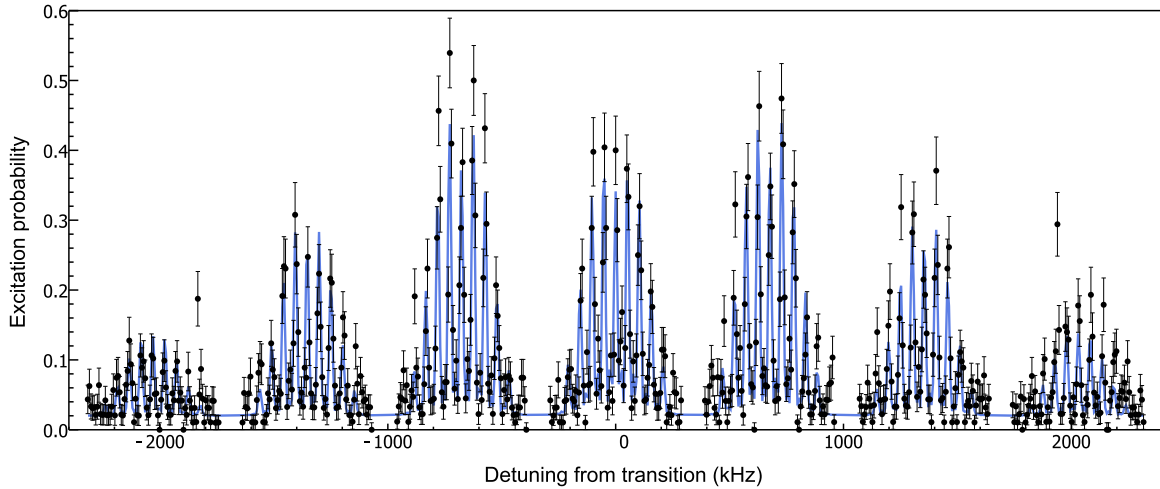
FIG. 7. Radial Doppler spectrum with $\omega_+ = 2\pi \times 677$ kHz, $\omega_- = 2\pi \times 52$ kHz taken with 1 V axialization. Full fit to two-mode Rabi dynamics gives the mean phonon numbers $\bar{n}_+ = 96(5)$ and $\bar{n}_- = 136(8)$ and $\Omega_0/2\pi = 26$ kHz. Radial laser parameters: $\delta \approx \Gamma/2$, $w_0 \approx 100$ $\mu$m, $y_0 \approx 80 - 120$ $\mu$m.

by approximately a factor of 9, while the modified cyclotron spectrum in panel (b) sees only a slight broadening. Thus the net effect of the axialization drive is the removal of over 800 phonons from the total radial motion while bringing the two phonon numbers close to equality.

To further confirm that axialization can be used to effectively cool at large trapping frequencies where resolved sideband cooling can be effectively employed, a data set at $\omega_- = 2\pi \times 52$ kHz and $V_{ax} = 1$ V is shown in Fig. 7 with all other parameters kept the same. At this frequency, cooling with just an offset beam is not possible. By fitting the full Rabi line-shape dynamics summed over a thermal distribution of phonons to three modified cyclotron and four magnetron sidebands, mean phonon numbers of $\bar{n}_+ = 96(5)$ and $\bar{n}_- = 136(8)$ were extracted. Once again, the mean phonon numbers approach equality, with the modified cyclotron being slightly lower (as predicted in Fig. 5); however, they are approximately a factor of 3 larger than the simulated values. One contribution to the discrepancy is that heating due to spontaneous emission from the axial cooling laser was omitted from the simulation. Based on the analytical model of modified cyclotron Doppler cooling, this effect could contribute up to 30% higher mean phonon numbers given a 1:1 scattering ratio of the radial and axial beams. The remaining discrepancy could be attributed to the uncertainty in setting the optimal laser parameters, including detuning, beam waist, and offset. Nonetheless, axialization allows us to cool the ion to low motional phonon numbers with high reliability and robustness against perturbations such as background gas collisions with only a modest applied voltage.

### 2. Sideband cooling

As the previous section demonstrated, with the aid of axialization we can consistently reach a regime with $\bar{n} \sim 100$ phonons in both modes at a magnetron frequency $\omega_- = 2\pi \times 52$ kHz, which is far outside the Lamb-Dicke regime ($\eta_r \sqrt{2\bar{n} + 1} \approx 2$, with $\eta_r$ being the same Lamb-Dicke parameter for both radial modes since it depends on the extent

of the radial motion wave packet, which is defined in terms of $\omega_1$ [36]). If we take the mean phonon number of $\bar{n}_- = 136(8)$ from Fig. 7, then we find that almost 25% of the thermal population is in Fock states above the first-order sideband coupling minimum at $n = 196$, thus clearly ruling out cooling on just first-order motional sidebands. Sideband cooling from outside the Lamb-Dicke regime is still possible but requires the addressing of higher-order motional sidebands to prevent any accumulation of population in any of the coupling minima. This has been shown previously in rf traps [55,56] as well as in our Penning trap for the axial motion of single ions [8] and small Coulomb crystals [50]. In fact, cooling the two axial modes of a two-ion chain at low trap frequency is similar to the problem of cooling the two radial modes of a single ion in that both require addressing higher-order sidebands of both motions in turn. However, in this case we need to address the blue sidebands of the magnetron motion rather than the red sidebands, as a consequence of the negative total energy of this motion. Following the approach to cooling sequence design for two modes of an ion chain outlined in Ref. [57], we adopt a 68-ms-long cooling sequence (Table I) that addresses the red modified cyclotron and blue magnetron sidebands. This sequence is not proven to be optimal but is tested to be experimentally robust and follows the philosophy that cooling is initially faster on higher-order sidebands, while the lowest order sidebands are required to reach the lowest mean phonon number. Furthermore, owing to the proximity of the first magnetron sideband to the carrier, the 729-nm laser Rabi frequency is lowered by approximately a factor of $\sqrt{2}$, and the effective upper state linewidth set by the quench laser is maintained at $\tilde{\Gamma}/2\pi = 5 - 10$ kHz to minimize unwanted off-resonant excitation of the carrier. Figure 7 suggests that sidebands that reduce the motional quanta of both modes could be initially used to cool both modes simultaneously when far outside the Lamb-Dicke regime, but this approach was not pursued here.

After applying the sequence outlined in Table I to an ion cooled with the same Doppler beam and trap parameters as in

TABLE I. A 68-ms sideband cooling sequence for both radial modes.

| Sideband | Pulse length (ms) | 729 Intensity (%) |
| --- | --- | --- |
| 2nd cyclotron | 5 | 100 |
| 1st cyclotron | 10 | 100 |
| 3rd magnetron | 5 | 100 |
| 2nd magnetron | 5 | 100 |
| 1st magnetron | 5 | 52 |
| 2nd cyclotron | 5 | 100 |
| 1st cyclotron | 5 | 100 |
| 3rd magnetron | 5 | 100 |
| 2nd magnetron | 5 | 100 |
| 1st magnetron | 5 | 52 |
| 1st cyclotron | 10 | 100 |
| 1st magnetron | 2 | 52 |
| 1st cyclotron | 1 | 100 |

Fig. 7, the spectrum shown in Fig. 8 is obtained. The strong suppression of the red modified cyclotron sideband and the asymmetry in the magnetron sidebands is evidence that a significant proportion of the population of both modes is in the ground state. A fit to the Rabi dynamics summed over a thermal Fock-state population results in phonon numbers of $\bar{n}_+ = 0.30(5)$ and $\bar{n}_- = 1.7(2)$. Furthermore, the spectrum of Fig. 8 shows no higher-order red magnetron sidebands, which would be expected if population were trapped at a coupling minimum. The red modified cyclotron sideband does
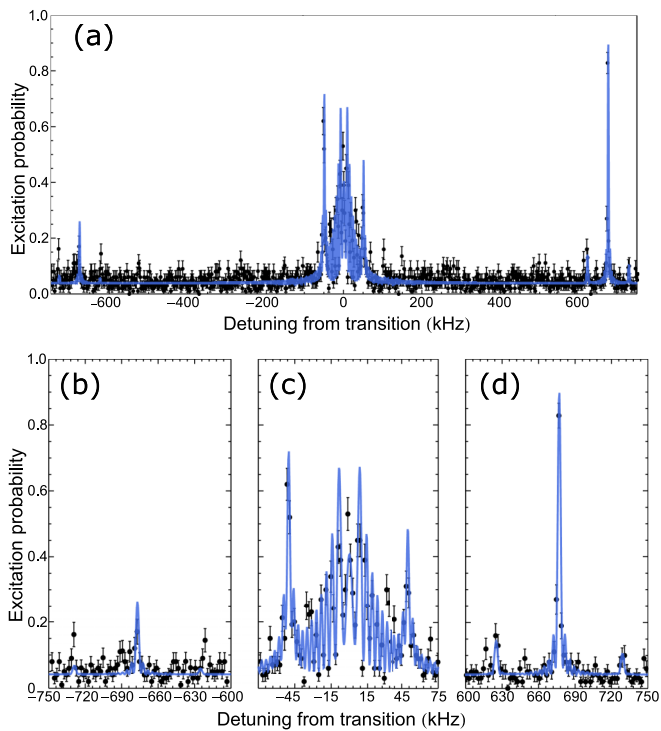


FIG. 8. (a) Continuous spectrum after 68 ms of sideband cooling (see Table I) with a probe time of 280 $\mu$s. Below, zoomed-in plots around (b) first red cyclotron sideband, (c) carrier with magnetron sidebands, and (d) first blue cyclotron sideband. Fit parameters using a two-mode thermal model: $\bar{n}_+ = 0.35(5)$, $\bar{n}_- = 1.7(2)$, $\Omega_0/2\pi = 14.13(4)$ kHz.
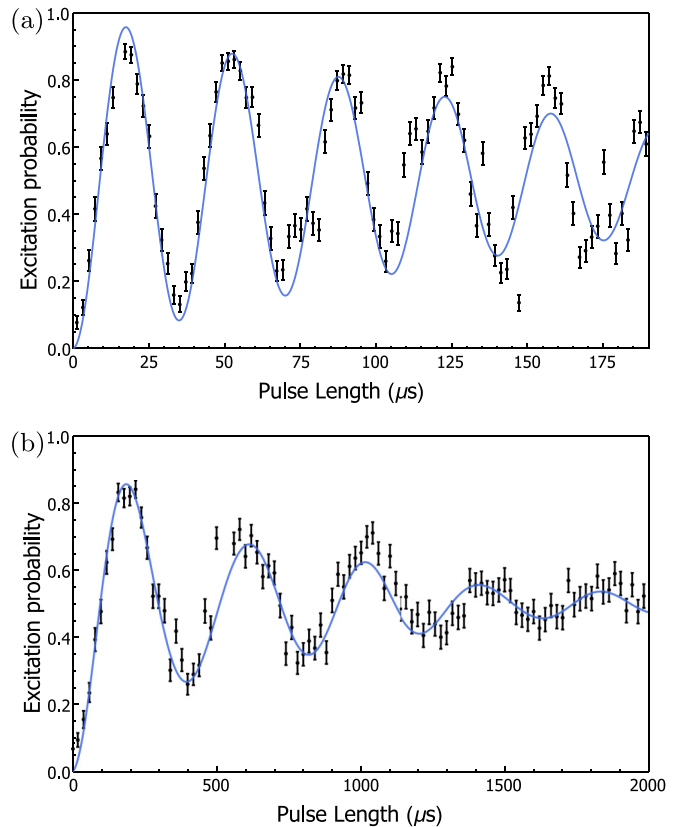


FIG. 9. Rabi oscillations after 68 ms of sideband cooling. (a) Carrier and (b) blue sideband modified cyclotron with fit parameters using a two-mode thermal model with fixed $\bar{n}_- = 1$: $\bar{n}_+ = 0.15(3)$, $\Omega_0/2\pi = 20.70(7)$ kHz.

appear to have two excess shelving events near $\omega_+ \pm \omega_-$; however, they are not consistent with a thermal model fit, nor can they represent trapped population in the magnetron coupling minima, as there is no evidence of corresponding magnetron sidebands around the carrier. An additional scan was later performed around the modified cyclotron sidebands where these events were not reproduced. Since the cooling sequence ends with a modified cyclotron pulse, the final value of $\bar{n}_-$ has an appreciable contribution from motional heating, which was separately measured to be $\approx$300 phonons s$^{-1}$. The motional heating is most likely to originate from technical noise on the dc supplies of the ring electrodes. The remaining excess thermal population of the magnetron mode arises from off-resonant carrier excitation and could be further suppressed by working at a higher magnetron frequency.

We also verify our ability to coherently drive the ion by performing Rabi oscillations on the carrier and the modified cyclotron blue sideband, shown in Fig. 9. The contrast of the carrier oscillations is limited by Cauchy-distributed Rabi frequency fluctuations of 3.1% extracted from an exponential decay of the visibility, with slow drifts on the timescale of a few seconds to minutes also causing measurement points at later times to lie several standard deviations away from the fit line. The source of this effect is believed to be polarization noise in the final 5-m-long optical fiber of the spectroscopy laser before the trap, with the transition sensitive to any drift away

from perfect linear polarization. Due to this noise, the carrier Rabi oscillation data cannot be used to accurately constrain the mean phonon numbers of the two modes as Rabi frequency components only depend weakly on $n$. On the other hand, the modified cyclotron Rabi oscillations will have frequency components that depend strongly on $\bar{n}_+$, and the decay line shape for a thermal distribution of $\bar{n}_+ \approx 1$ can be distinguished from an exponential decay induced by fast Rabi frequency noise. Using a fit to the two-mode Rabi excitation formula,

$$P_e(t) = \sum_{n_+,n_-}^{15} \frac{\bar{n}_+^{n_+}}{(\bar{n}_+ + 1)^{n_+ + 1}} \frac{\bar{n}_-^{n_-}}{(\bar{n}_- + 1)^{n_- + 1}}$$

$$\times \frac{1}{2}\left(1 - e^{-t/\tau_e} \cos \Omega_{n_+,n_++1}^{n_-,n_-} t\right), \qquad (25)$$

with the generalized Rabi frequency $\Omega_{n_+,n_++1}^{n_-,n_-}$ phonon dependence incorporated using the full Laguerre polynomial dependence [58] and an exponential decay time constant $\tau_e$, the data suggests $\bar{n}_+ = 0.15(3)$ for fixed $\bar{n}_-$ of 1. The decay constant of $\tau_e = 780(40)$ $\mu$s corresponds to a generalized Rabi frequency noise of 10%, which is consistent with the polarization fluctuations described above as well as additional broadening due to the laser linewidth of 1.6(1) kHz. This linewidth is consistent with independent Ramsey spectroscopy measurements of the qubit transition coherence time of $\approx 600$ $\mu$s.

## IV. CONCLUSION

In this article we have presented experimental results of sideband cooling showing significant occupation of the ground states of motion of both radial modes of a single ion in a Penning trap. Due to the negative energy of the magnetron motion, blue motional sidebands were excited in order to remove motional quanta. On the other hand, the modified cyclotron was cooled in the conventional manner by targeting red motional sidebands. As a prerequisite for this result, we experimentally show how the use of an axialization drive, providing a resonant mode coupling, works in conjunction with a radially offset Doppler cooling beam to effectively reduce the mean phonon number of the magnetron motion to values amenable to sideband cooling. Furthermore, we numerically study the parameter space of Doppler cooling and show that with modest applied axialization voltage, low mean phonon numbers of both modes can be attained.

Coherent control of a ground-state-cooled ion is demonstrated by showing Rabi flops on the carrier and blue sideband transitions. The studies are useful for future Penning-trap-based high-precision and quantum simulation experiments, where the unwanted effects due to occupation in motional states can be minimized by performing sideband cooling.

[1] F. Diedrich, J. C. Bergquist, W. M. Itano, and D. J. Wineland, Phys. Rev. Lett. **62**, 403 (1989).

[2] C. Monroe, D. M. Meekhof, B. E. King, S. R. Jefferts, W. M. Itano, D. J. Wineland, and P. Gould, Phys. Rev. Lett. **75**, 4011 (1995).

[3] L. Deslauriers, P. C. Haljan, P. J. Lee, K.-A. Brickman, B. B. Blinov, M. J. Madsen, and C. Monroe, Phys. Rev. A **70**, 043408 (2004).

[4] H. Che, K. Deng, Z. T. Xu, W. H. Yuan, J. Zhang, and Z. H. Lu, Phys. Rev. A **96**, 013417 (2017).

[5] B. E. King, C. S. Wood, C. J. Myatt, Q. A. Turchette, D. Leibfried, W. M. Itano, C. Monroe, and D. J. Wineland, Phys. Rev. Lett. **81**, 1525 (1998).

[6] R. Lechner, C. Maier, C. Hempel, P. Jurcevic, B. P. Lanyon, T. Monz, M. Brownnutt, R. Blatt, and C. F. Roos, Phys. Rev. A **93**, 053401 (2016).

[7] Y. Lin, J. P. Gaebler, T. R. Tan, R. Bowler, J. D. Jost, D. Leibfried, and D. J. Wineland, Phys. Rev. Lett. **110**, 153002 (2013).

[8] J. F. Goodwin, G. Stutter, R. C. Thompson, and D. M. Segal, Phys. Rev. Lett. **116**, 143002 (2016).

[9] E. Jordan, K. A. Gilmore, A. Shankar, A. Safavi-Naini, J. G. Bohnet, M. J. Holland, and J. J. Bollinger, Phys. Rev. Lett. **122**, 053603 (2019).

[10] T. Monz, D. Nigg, E. A. Martinez, M. F. Brandl, P. Schindler, R. Rines, S. X. Wang, I. L. Chuang, and R. Blatt, Science **351**, 1068 (2016).

[11] A. Bermudez, X. Xu, R. Nigmatullin, J. O'Gorman, V. Negnevitsky, P. Schindler, T. Monz, U. G. Poschinger, C. Hempel, J. Home, F. Schmidt-Kaler, M. Biercuk, R. Blatt, S. Benjamin, and M. Müller, Phys. Rev. X **7**, 041061 (2017).

[12] N. M. Linke, D. Maslov, M. Roetteler, S. Debnath, C. Figgatt, K. A. Landsman, K. Wright, and C. Monroe, Proc. Natl. Acad. Sci. **114**, 3305 (2017).

[13] K. Kim, M.-S. Chang, S. Korenblit, R. Islam, E. E. Edwards, J. K. Freericks, G.-D. Lin, L.-M. Duan, and C. Monroe, Nature (London) **465**, 590 (2010).

[14] J. T. Barreiro, M. Müller, P. Schindler, D. Nigg, T. Monz, M. Chwalla, M. Hennrich, C. F. Roos, P. Zoller, and R. Blatt, Nature (London) **470**, 486 (2011).

[15] B. P. Lanyon, C. Hempel, D. Nigg, M. Muller, R. Gerritsma, F. Zahringer, P. Schindler, J. T. Barreiro, M. Rambach, G. Kirchmair, M. Hennrich, P. Zoller, R. Blatt, and C. F. Roos, Science **334**, 57 (2011).

[16] S. Korenblit, D. Kafri, W. C. Campbell, R. Islam, E. E. Edwards, Z.-X. Gong, G.-D. Lin, L.-M. Duan, J. Kim, K. Kim, and C. Monroe, New J. Phys. **14**, 095024 (2012).

[17] E. A. Martinez, C. A. Muschik, P. Schindler, D. Nigg, A. Erhard, M. Heyl, P. Hauke, M. Dalmonte, T. Monz, P. Zoller, and R. Blatt, Nature (London) **534**, 516 (2016).

[18] G. Araneda, D. B. Higginbottom, L. Slodička, Y. Colombe, and R. Blatt, Phys. Rev. Lett. **120**, 193603 (2018).

[19] P. O. Schmidt, T. Rosenband, C. Langer, W. M. Itano, J. C. Bergquist, and D. J. Wineland, Science **309**, 749 (2005).

[20] W. M. Itano and D. J. Wineland, Phys. Rev. A **25**, 35 (1982).

[21] K. Blaum, Y. N. Novikov, and G. Werth, Contemp. Phys. **51**, 149 (2010).

[22] D. Hanneke, S. Fogwell, and G. Gabrielse, Phys. Rev. Lett. **100**, 120801 (2008).

[23] J. DiSciacca and G. Gabrielse, Phys. Rev. Lett. **108**, 153001 (2012).

[24] H. Nagahama, C. Smorra, S. Sellner, J. Harrington, T. Higuchi, M. J. Borchert, T. Tanaka, M. Besirli, A. Mooser, G. Schneider, K. Blaum, Y. Matsuda, C. Ospelkaus, W. Quint, J. Walz, Y. Yamazaki, and S. Ulmer, Nat. Commun. **8**, 14084 (2017).

[25] S. Schmidt, T. Murböck, Z. Andelkovic, G. Birkl, K. König, W. Nörtershäuser, R. C. Thompson, and M. Vogel, J. Mod. Opt. **65**, 538 (2018).

[26] M. Bohman, A. Mooser, G. Schneider, N. Schön, M. Wiesinger, J. Harrington, T. Higuchi, H. Nagahama, C. Smorra, S. Sellner, K. Blaum, Y. Matsuda, W. Quint, J. Walz, and S. Ulmer, J. Mod. Opt. **65**, 568 (2018).

[27] T. Meiners, M. Niemann, A.-G. Paschke, J. Mielke, A. Idel, M. Borchert, K. Voges, A. Bautista-Salvador, S. Ulmer, and C. Ospelkaus, J. Phys. Soc. Jpn. **18**, 1 (2016).

[28] J. W. Britton, B. C. Sawyer, A. C. Keith, C. C. J. Wang, J. K. Freericks, H. Uys, M. J. Biercuk, and J. J. Bollinger, Nature (London) **484**, 489 (2012).

[29] J. G. Bohnet, B. C. Sawyer, J. W. Britton, M. L. Wall, A. M. Rey, M. Foss-Feig, and J. J. Bollinger, Science **352**, 1297 (2016).

[30] J. F. Goodwin, B. J. Brown, G. Stutter, H. Dale, R. C. Thompson, and T. Rudolph, Phys. Rev. A **92**, 032314 (2015).

[31] S. B. Torrisi, J. W. Britton, J. G. Bohnet, and J. J. Bollinger, Phys. Rev. A **93**, 043421 (2016).

[32] C. Tang, D. Meiser, J. J. Bollinger, and S. E. Parker, Phys. Plasmas **26**, 073504 (2019).

[33] H. G. Dehmelt, Adv. At., Mol., Opt. Phys. **3**, 53 (1968).

[34] L. S. Brown and G. Gabrielse, Rev. Mod. Phys. **58**, 233 (1986).

[35] M. Kretzschmar, Eur. J. Phys. **12**, 240 (1991).

[36] F. Crimin, B. M. Garraway, and J. Verdú, J. Mod. Opt. **65**, 427 (2018).

[37] G. Z. K. Horvath and R. C. Thompson, Phys. Rev. A **59**, 4530 (1999).

[38] R. C. Thompson and J. Papadimitriou, J. Phys. B: At., Mol. Opt. Phys. **33**, 3393 (2000).

[39] S. Mavadia, J. F. Goodwin, G. Stutter, S. Bharadia, D. R. Crick, D. M. Segal, and R. C. Thompson, Nat. Commun. **4**, 2571 (2013).

[40] D. Wineland and H. Dehmelt, Int. J. Mass Spectrom. Ion Phys. **16**, 338 (1975).

[41] R. S. Van Dyck, P. B. Schwinberg, and H. G. Dehmelt, Phys. Rev. Lett. **38**, 310 (1977).

[42] E. A. Cornell, R. M. Weisskoff, K. R. Boyce, and D. E. Pritchard, Phys. Rev. A **41**, 312 (1990).

[43] G. Bollen, R. B. Moore, G. Savard, and H. Stolzenberg, J. Appl. Phys. **68**, 4355 (1990).

[44] L. Schweikhard and A. G. Marshall, J. Am. Soc. Mass Spectrom. **4**, 433 (1993).

[45] D. J. Wineland and W. M. Itano, Phys. Rev. A **20**, 1521 (1979).

[46] H. F. Powell, D. M. Segal, and R. C. Thompson, Phys. Rev. Lett. **89**, 093003 (2002).

[47] H. F. Powell, S. R. d. Echaniz, E. S. Phillips, D. M. Segal, and R. C. Thompson, J. Phys. B: At., Mol. Opt. Phys. **36**, 961 (2003).

[48] E. S. Phillips, R. J. Hendricks, A. M. Abdulla, H. Ohadi, D. R. Crick, K. Koo, D. M. Segal, and R. C. Thompson, Phys. Rev. A **78**, 032307 (2008).

[49] D. R. Crick, H. Ohadi, I. Bhatti, R. C. Thompson, and D. M. Segal, Opt. Express **16**, 2351 (2008).

[50] G. Stutter, P. Hrmo, V. Jarlaud, M. K. Joshi, J. F. Goodwin, and R. C. Thompson, J. Mod. Opt. **65**, 549 (2018).

[51] G. Stutter, Ph.D. thesis, Imperial College London, 2015.

[52] R. J. Hendricks, E. S. Phillips, D. M. Segal, and R. C. Thompson, J. Phys. B: At., Mol. Opt. Phys. **41**, 035301 (2008).

[53] S. Jain, J. Alonso, M. Grau, and J. P. Home, arXiv:1812.06755.

[54] D. R. Crick, S. Donnellan, D. M. Segal, and R. C. Thompson, Phys. Rev. A **81**, 052503 (2010).

[55] G. Morigi, J. Eschner, J. I. Cirac, and P. Zoller, Phys. Rev. A **59**, 3797 (1999).

[56] G. Poulsen, Y. Miroshnychenko, and M. Drewsen, Phys. Rev. A **86**, 051402(R) (2012).

[57] M. K. Joshi, P. Hrmo, V. Jarlaud, F. Oehl, and R. C. Thompson, Phys. Rev. A **99**, 013423 (2019).

[58] D. Wineland, C. Monroe, W. Itano, B. King, D. Leibfried, D. Meekhof, C. Myatt, and C. Wood, Fortschr. Phys. **46**, 363 (1998).